scientific reports

Check for updates

OPEN

TRIM21 knockdown alleviates hemorrhage induced hepatic ischemia reperfusion injury by suppressing ferroptosis-induced NETs

Shikai Wang[1,2], Zhipeng Li[1,2], Yunxiang Chang[1], Di He[1], Kai Dong[1] & Xinsheng Cheng[1]✉

Hemorrhage-induced hepatic ischemia/reperfusion (I/R) injury is a severe complication of hemorrhagic shock, yet its molecular mechanisms remain unclear. The aim of this study was to investigate the potential mechanism of action of TRIM21 on hemorrhage-induced hepatic I/R injury. The role of TRIM21 in hepatic I/R injury was evaluated by establishing a mouse model of hemorrhage-induced hepatic I/R injury and an in vitro simulated oxygen–glucose deprivation/reoxygenation (OGD/R) hepatocyte injury model. A comprehensive analysis was conducted, including histopathological changes, serum biochemical indicators, inflammatory cytokine levels, markers of neutrophil extracellular trap (NETs) formation, and biomarkers related to ferroptosis, such as the expression of iron metabolism-related proteins SLC7A11 and FTH1, oxidative stress and antioxidant capacity, NETs formation markers (Cit-H3, PAD4, and MPO), and the expression levels of TRIM21.The study revealed that ferroptosis-induced NETs was involved in the process of hepatic I/R injury, concurrent with elevated serum ALT and AST levels and increased cell apoptosis. In the hemorrhage-induced hepatic I/R injury mouse model and OGD/R-induced hepatocyte injury, the expression of TRIM21 is significantly upregulated. Knockdown of TRIM21 can effectively inhibit the formation of ferroptosis-induced NETs, thereby alleviating hepatic I/R injury. In terms of the underlying mechanism, TRIM21 promotes the formation of ferroptosis-induced NETs by regulating the stability of the SLC7A11 protein, thus exacerbating hepatic I/R injury. The study discovered that silencing TRIM21 inhibits ferroptosis-mediated NETs formation by ubiquitinating SLC7A11, effectively alleviating hepatic I/R injury. This discovery may provide a potential therapeutic strategy for the treatment of hemorrhage-induced hepatic I/R injury.

Keywords Hemorrhage-induced hepatic ischemia/reperfusion injury, NETs, TRIM21, Ferroptosis, SLC7A11

Hemorrhagic shock is a common clinical emergency. When the body goes into shock, the liver, as a vital organ with rich blood supply, is highly susceptible to ischemia and hypoxia leading to functional failure. Rapid hemostasis and fluid resuscitation are crucial steps in the rescue process. However, these steps are also significant contributors to the occurrence of hepatic ischemia–reperfusion injury[1,2]. Hepatic ischemia/reperfusion (I/R) injury is defined as liver injury due to ischemia and subsequent reperfusion after hepatic blood flow is restored. The occurrence of hepatic I/R can be divided into two phases: ischemic injury and reperfusion injury[3,4]. In the ischemic stage, hepatocytes are damaged by hypoxia due to the cessation of blood flow; whereas in the reperfusion stage, when blood flow is restored, hepatocytes that have already been damaged are further damaged. Specifically, the massive production of oxygen free radicals, calcium overload, Kupffer cell activation, inflammatory response, and mitochondrial dysfunction during reperfusion combine to exacerbate hepatocellular injury. IR inflicts hepatic tissue damage by diminishing ATP supply, triggering a surge in ROS, amplifying inflammatory reactions, and instigating cellular demise[5–7]. Therefore, understanding the pathogenesis of I/R and identifying potential therapeutic targets are of paramount clinical importance, as is the exploration of new treatment approaches for I/R.

[1]Department of Hepatobiliary Pancreas Surgery, Shenzhen Nanshan District People's Hospital, NO.89 Taoyuan Road, Nanshan District, Shenzhen 518052, Guangdong Province, China. [2]Shikai Wang and Zhipeng Li have contributed equally to this work. ✉email: shenzhenhos_21@sina.com

Neutrophils, a crucial component of the immune system and the most abundant type of white blood cell in the bloodstream, play a significant role in innate and adaptive immunity[8,9]. Neutrophils in their activated state are capable of producing and releasing neutrophil extracellular traps (NETs), a long filamentous extracellular meshwork of depolymerized DNA, together with guanosine histone H3, neutrophil elastase (NE), histone G, and myeloperoxidase (MPO)[10]. NETs have antimicrobial and antiviral properties in inflammatory responses, but excessive NETs formation and deposition can lead to tissue damage[11–13]. Latest research shows that the formation of NETs is closely related to the pathogenesis of intestinal, liver, and lung injuries in I/R diseases. In diseases such as acute lung injury and cerebrovascular dysfunction, excessive production of NETs has been proven to exacerbate pathological conditions[14–17]. Ferroptosis, characterized by its reliance on iron-dependent lipid peroxidation, has been intimately linked with a multitude of cardiovascular disorders[18,19]. Recent research indicates that I/R can induce ferroptosis in affected tissues. For example, in an I/R model of acute kidney injury, morphological changes caused by ferroptosis in renal tubular epithelial cells were observed. The application of ferroptosis inhibitors has been shown to significantly alleviate kidney damage and partially reverse the process of ferroptosis[20,21]. Moreover, these inhibitors have also been proven to suppress liver injury and lipid peroxidation in mouse models of hepatic I/R injury. These research findings suggest that the inhibition of ferroptosis may serve as an effective strategy for treating I/R injury[22,23]. It is worth noting that the formation process of NETs is mainly dependent on the production of reactive oxygen species (ROS), which shares a similar biological basis in the process of ferroptosis. Although ferroptosis and NETs have similarities in intracellular signaling pathways, their interrelationship during liver I/R remains unclear.

Tripartite motif-containing 21 (TRIM21), as an E3 ubiquitin ligase, belongs to the TRIM (Tripartite motif) protein family and is involved in a variety of biological processes within the cell, including redox homeostasis, apoptosis and inflammatory responses[24]. TRIM21 is expressed across a variety of tissues, with notably elevated levels observed in the cardiac and immune systems[25]. Recent research has revealed a novel form of cell death known as ferroptosis in heart disease. Ferroptosis plays a significant role in cardiac diseases such as myocardial ischemia–reperfusion injury and doxorubicin-induced cardiomyopathy, and the specific inhibition of ferroptosis can alleviate cardiac damage[26,27]. Studies have found that the absence of TRIM21 can mitigate cardiac toxicity by suppressing doxorubicin-induced ferroptosis. The mechanism of interaction between TRIM21 and FSP1 and its impact on the resistance of tumor cells to ferroptosis have also been a focus of research[28,29]. However, it is unclear whether TRIM21 regulates hepatic I/R injury. Therefore, in this study, we aim to explore the regulatory role of TRIM21 in hepatic I/R injury by modulating the formation of ferroptosis-induced NETs.

Materials and methods

Hemorrhage-induced hepatic I/R model

C57BL/6 mice (8–10 weeks old, 25–30 g) were purchased from Guangzhou RuiGe Biotechnology Co., Ltd. They were housed in cages with standard conditions and maintained on a 12-h light/dark cycle while ensuring that they were able to eat and drink freely. The mice were randomly divided into control group (n = 5), I/R group (n = 5), I/R + DNase-1 group (n = 5), I/R + Fer-1 treatment group (n = 5), I/R + AAV + si-NC group (n = 5), and I/R + AAV + si-TRIM21 group (n = 5). To eliminate interference, all experimental groups had corresponding control groups. All animal procedures are conducted in accordance with the Guide for the Care and Use of Laboratory Animals published by the National Institutes of Health and are approved by the Animal Management Committee of Nanshan people's Hospital. We confirmed that all methods were carried out under relevant guidelines and regulations. Moreover, we confirmed that all methods are reported following ARRIVE guidelines (https://arriveguidelines.org).

We anesthetized mice with intraperitoneal injection of 3% pentobarbital sodium, after anesthesia was administered to the C57BL/6 mice, they were placed on the operating table, and the mice were cannulated through the common carotid artery and jugular vein. The process of hemorrhagic shock was simulated by slow bloodletting through the common carotid artery cannulation. After successful induction of hemorrhagic shock, the hepatic artery and portal vein vessels were rapidly clamped to render the liver ischemic. After 90 min of ischemia, the vascular clamps and other devices were released to restore the blood supply to the liver, and then the reperfusion began for 6 h. Immediately after the end of reperfusion, serum and liver samples were collected. Sham-operated mice underwent the same surgical procedure without occlusion of the vascular system. The mice were euthanized by intraperitoneal injection of 3% pentobarbital sodium at the end of the study.

Cell culture and treatment

LO2 cells (IM-H043, Immocell, China) were cultured in DMEM medium containing 10% fetal bovine serum and 1% penicillin–streptomycin at 37 °C and 5% CO_2 in a cell culture incubator. To establish the Oxygen–Glucose Deprivation/Reoxygenation (OGD/R) model, the LO2 cells were first placed in a hypoxic incubator (containing 5% CO_2 and 95% N_2) for a 4-h incubation. Subsequently, the cells were transferred to a normoxic environment with 95% air and 5% CO_2, and continued to be incubated in complete DMEM medium for 12 h for reoxygenation.

Biochemical analysis

Serum are obtained by centrifuging the blood samples. Serum aspartate aminotransferase (AST) and alanine aminotransferase (ALT) kits (C010-2–1, C009-2-1, Jiancheng Bioengineering Institute, Nanjing, China) were used to test AST and ALT levels to assess hepatic functional status according to the manufacturer's guidelines.

Histology and TUNEL analysis

Samples were fixed in 4% paraformaldehyde, paraffin-embedded and cut into thin slices for hematoxylin and eosin staining to assess the extent of liver injury. Following the manufacturer's instructions, the terminal

deoxynucleotidyl transferase-mediated dUTP nick end labeling (TUNEL) staining kit (C1088, Beyotime, China) was used to evaluate hepatocyte apoptosis.

Measurement of MDA, GSH, SOD, and ROS

Following the manufacturer's instructions, quantitative analysis of malondialdehyde (MDA, E-EL-0060, Elabscience, China), glutathione (GSH, E-EL-0026, Elabscience, China), and superoxide dismutase (SOD, E-EL-H6188, Elabscience, China) levels in the samples is performed using the Enzyme-Linked Immunosorbent Assay (ELISA) method. The levels of reactive oxygen species (ROS) within cells were quantified utilizing a ROS Assay Kit The levels of reactive oxygen species (ROS) within cells were quantified utilizing a ROS Assay Kit (S0033S, Beyotime Biotechnology, China).

Immunohistochemistry

The tissue sections were processed with 3% H2O2 to inhibit the activity of endogenous peroxidases. Subsequently, the sections were blocked with 10% bovine serum albumin (BSA) for 1 h to minimize background staining. The slides were then incubated overnight at 4 °C with SLC7A11 antibody (1:1000, 26864-1-AP, Proteintech Group) and GPX4 antibody (1:5000, 67763-1-Ig, Proteintech Group) to bind to the target antigens. After incubation, the sections were washed with PBS to remove any unbound primary antibodies. HRP-conjugated secondary antibodies were added, and the sections were incubated for an additional 30 min at room temperature to amplify the signal. Following the secondary antibody incubation, the slides were developed with DAB (3,3'-diaminobenzidine) and counterstained with hematoxylin. Finally, the stained sections were observed under a microscope (Olympus, Tokyo, Japan) for evaluation of antigen expression.

Immunofluorescence staining

The samples were fixed with 4% paraformaldehyde and then washed with PBS to remove excess fixative. Next, the sectioned samples were blocked with BSA and then incubated with specific primary antibodies (anti- MPO (1:100, ab208670, Abcam, USA), anti- TRIM21 (1:800, 67136-1-Ig, Proteintech, China), anti- SLC7A11 (1:1000, 26864-1-AP, Proteintech, China)) at 4 °C overnight. After washing the sections, fluorescently labeled secondary antibodies that bind specifically to the primary antibodies were added and incubated for 1 h at room temperature. Finally, the nuclei were stained using DAPI dye (STC448, Seyotin, China). The sections were observed under a fluorescence microscope (OLYMPUS) and quantitatively analyzed using image analysis software.

Co-immunoprecipitation (Co-IP)

The cells were lysed under non-denaturing conditions to maintain the integrity of the protein structure and antigen. Next, the SLC7A11 antibody was mixed thoroughly with the cell lysate to form an immune complex. Subsequently, protein A/G agarose beads were added to the mixture to promote the formation of a stable complex between the antibody-antigen and the beads. The complexes were separated using SDS-PAGE electrophoresis. After electrophoresis, proteins were transferred to the membrane and analyzed by Western blotting using SLC7A11 antibody (1:1000, 26864-1-AP, Proteintech Group) or TRIM21 antibody (1:5000, 67136-1-Ig, Proteintech Group).

Real-time PCR analysis

Total RNA was extracted from liver cells and tissues by Trizol reagent (SYT010, Seyotin, China). Subsequently, the extracted RNA was converted into cDNA by reverse transcription reaction. When configuring the qPCR reaction system, cDNA templates, primers (in Table 1), and tests such as qPCR Master Mix (SYT103, Seyotin, China) were precisely added. Next, the qPCR amplification reaction was carried out by setting the appropriate reaction conditions on the qPCR instrument, and the target genes were quantitatively analyzed using the $2^{-\Delta\Delta CT}$ method.

Western blot analysis

Liver tissues and cells are mixed with lysis buffer and undergo homogenization and lysis treatment. Next, the protein concentration in the lysate is determined using a BCA protein assay kit (P0012S, Beyotime, Shanghai, China). The prepared protein samples are then loaded onto an SDS-PAGE gel to separate proteins by molecular weight through electrophoresis. After electrophoresis, the proteins on the gel are transferred onto a PVDF

Genes	Forward (5′-3′)	Reverse (5′-3′)
IL-1β	GCTACCTGTGTCTTTCCCGT	CGTCACACACCAGCAGGTTA
IL-6	ATACCACTTCACAAGTCGGAGG	TGCAAGTGCATCATCGTTGTTC
TNF-α	AAGTGGAGGAGCAGCTGGAG	GCAGCCTTGTCCCTTGAAGA
CCL2	GATCCCAATGAGTAGGCTGGAG	TGTCTGGACCCATTCCTTCTTG
CCL5	GTGCCCACGTCAAGGAGTAT	TCTTCTCTGGGTTGGCACAC
CXCL2	CCTGCCAAGGGTTGACTTCA	GGCTTCAGGGTCAAGGCAAA
TRIM21	GGAGAAGATCCACGTGGCTT	GCGAACTCTGCGTGAATCCT
GAPDH	CTGATGCCCCCATGTTCGTC	CAGGGGTGCTAAGCAGTTGG

Table 1. Primer sequences.

membrane, which is then blocked with a 5% non-fat milk solution. The membrane is incubated overnight at 4 °C with specific primary antibodies (anti-Cit-H3 (1:2000, ab281584, Abcam, USA), anti-PAD4 (1:1000, ab214810, Abcam, USA), anti-SLC7A11 (1:1000, 26864-1-AP, Proteintech, China), anti-FTH1 (1:1000, ab183781, Abcam, USA), anti-GPX4 (1:5000, 67763-1-Ig, Proteintech, China), anti-IL-1β (1:1000, ab254360, Abcam, USA), anti-IL-6 (1:1000, ab259341, Abcam, USA), anti-TNF-α (1:2000, ab183218, Abcam, USA), anti-CCL2 (1:2000, 26161-1-AP, Proteintech, China), anti-CCL5 (1:1000, A14192, ABclonal, China), anti-CXCL2 (1:500, 26791-1-AP, Proteintech, China), anti-GAPDH (1:5000, ab181602, Abcam, USA)), allowing the antibodies to bind to their target proteins. After incubation, the membrane is washed with TBST buffer to remove unbound antibodies. Then, an HRP-conjugated secondary antibody is added, followed by another round of washing with TBST buffer. Finally, protein bands are detected using a chemiluminescent kit (P0018, Beyotime, Shanghai, China), and the expression of target protein was analyzed by comparing the target protein bands with the internal reference protein bands.

Statistical analysis

All data were analyzed by GraphPad Prism software and presented as mean ± standard deviation (SD), and each experiment was repeated at least three times independently. Statistical analyses were performed using one-way analysis of variance (ANOVA) with $P < 0.05$ as the criterion for determining statistical significance.

Results

NETs participating in hepatic I/R injury

In a mouse model of hepatic I/R injury, HE staining revealed significant tissue damage in the liver (Fig. 1A). Serum biochemical analysis demonstrated that levels of ALT and AST were substantially elevated in the hepatic I/R injury group compared to the control group (Fig. 1B–C). TUNEL assays detected an increase in apoptotic hepatocytes (Fig. 1D). Research has shown that PAD4 is essential for the formation of NETs. In activated neutrophils, the generation of ROS and calcium influx trigger the movement of PAD4 from the cytoplasm to the nucleus. This translocation leads to the citrullination of histones associated with DNA, resulting in DNA decondensation. The use of broad-spectrum PAD inhibitors to chemically inhibit PAD4 can effectively prevent NETosis, indicating that PAD4-induced histone citrullination is a critical step in NET formation[30]. The presence of citrullinated histones serves as a marker for the formation of NETs[31]. Western blot analysis revealed increased expression levels of Cit-H3 and PAD4 in hepatic I/R injury (Fig. 1E). Additionally, MPO, an important protein in the formation of NETs, was found to be significantly higher in the hepatic I/R injury group by immunofluorescence detection (Fig. 1F). qPCR detected elevated levels of key inflammatory and chemokine factors (IL-1β, IL-6, TNF-α, CCL2, CCL5, and CXCL2) in hepatic I/R injury (Fig. 1G). After DNase-I treatment, Western blot analysis showed a decrease in the expression levels of Cit-H3 and PAD4 (Fig. 1H). Further TUNEL assays and qPCR analysis found that hepatocyte injury and inflammatory factors in the hepatic I/R injury group were alleviated after DNase-I treatment (Fig. 1I–J).

Ferroptosis-induced NETs promote hepatic I/R injury

In order to explore the role of ferroptosis in hepatic I/R injury, a panel of ferroptosis biomarkers was assessed, encompassing the expression of proteins implicated in ferroptosis such as SLC7A11 and FTH1, alongside measurements of antioxidant activity markers (MDA, SOD, GSH) and the expression levels of GPX4. As shown in Fig. 2, MDA levels were elevated while SOD and GSH levels were decreased in the hepatic I/R injury group compared with the control group (Fig. 2A), while SLC7A11 and FTH1 protein expression was decreased (Fig. 2B). The results of immunohistochemistry showed that the expression of Gpx4 was also reduced (Fig. 2C). After the administration of FER-1 treatment, SOD and GSH levels were found to rebound and MDA levels were decreased (Fig. 2D–F). In addition, Western blotting and immunohistochemical analyses showed that the expression levels of SLC7A11, FTH1, and GPX4 were restored in the FER-1 treatment group (Fig. 2G–H).

TRIM21 facilitated the ferroptosis process

In this study, we examined the expression of TRIM21 in tissues. The results showed that the expression level of TRIM21 was significantly higher in the hepatic I/R injury group than in the control group (Fig. 3A–B). Next, we constructed an animal model of AAV-mediated hepatic I/R injury to investigate the effect of TRIM21 gene silencing on ferroptosis. The experimental results revealed that, compared to the control group, the levels of MDA were significantly increased, while the level of SOD and GSH were significantly reduced in the hepatic I/R injury group. Meanwhile the expression of SLC7A11, FTH1 and GPX4 was also significantly changed. Notably, by knocking down the expression of TRIM21, we found that MDA levels were decreased, while SOD and GSH activity was significantly elevated (Fig. 3C). In addition, the expression levels of SLC7A11, GPX4 and FTH1 were also elevated (Fig. 3D–E).

Knockdown of TRIM21 can inhibit the formation of NETs mediated by ferroptosis in the OGD/R model

By qPCR and immunofluorescence techniques, we detected the expression level of TRIM21 in cells and observed that in the OGD/R model group, the expression level of TRIM21 was significantly higher than that in the control group (Fig. 4A–B). To further investigate the effect of TRIM21 in ferroptosis, we knocked down the expression of TRIM21 using siRNA transfection and found that the key indicators of ferroptosis were significantly changed. Compared with the control group, the ROS content was increased in the OGD/R model group, whereas a significant reduction in ROS content was found by knocking down TRIM21 (Fig. 4C). In addition, we assessed the expression of antioxidant activity indicators such as MDA, SOD, GSH, as well as the ferroptosis-related proteins SLC7A11, FTH1, and GPX4, which aligned with the expression trend of TRIM21 in the tissue (Fig. 4D–

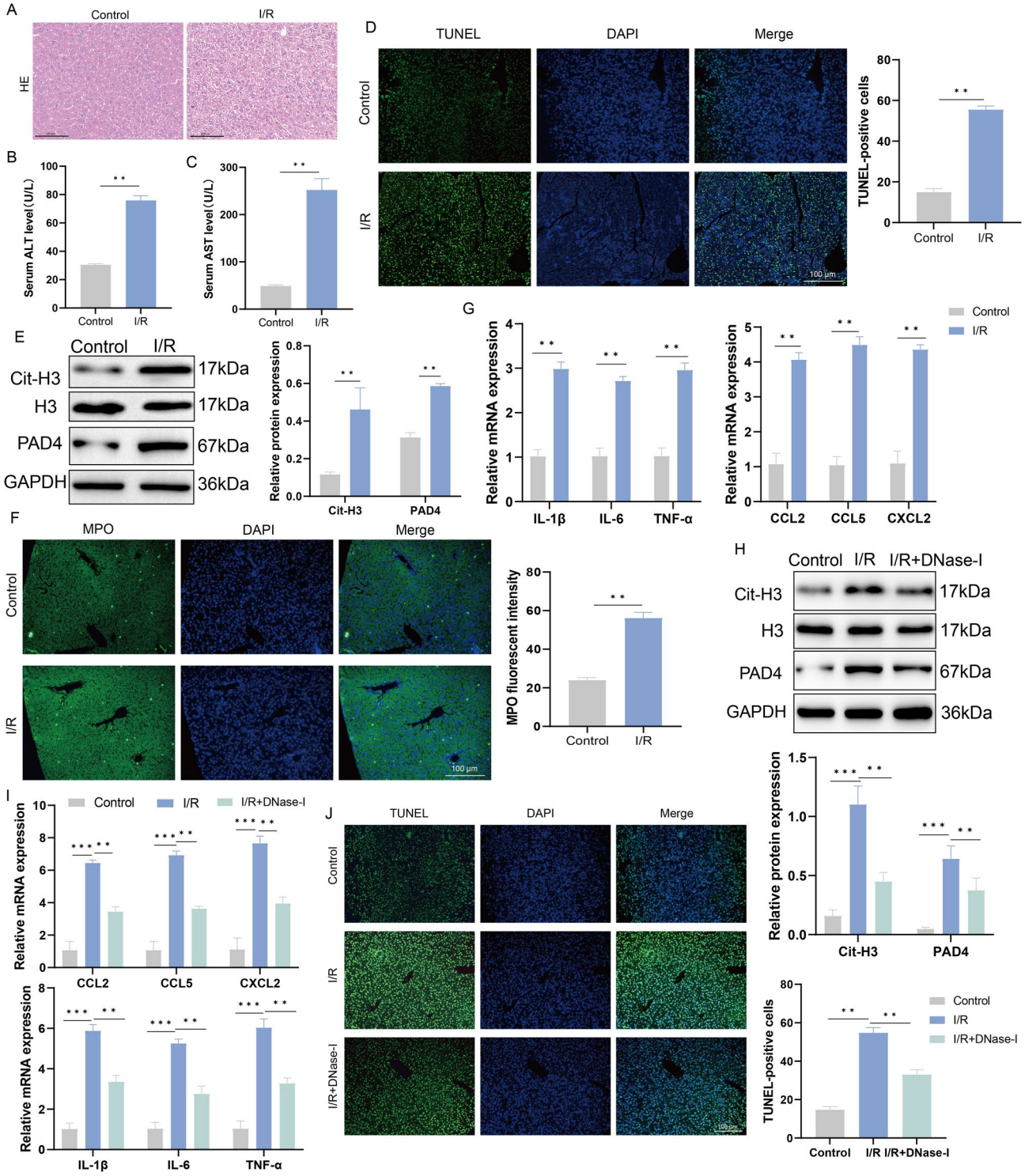

Fig. 1. NETs Participating in hepatic I/R injury. (**A**) HE staining. (**B**–**C**) Serum levels of ALT and AST. (**D**) Representative images of TUNEL staining in liver tissue and Quantitative analysis of TUNEL staining. (**E**) Western blot analysis of Cit-H3 and PAD4 protein content. (**F**) Immunofluorescence analysis of MPO content. Original blot is presented in Supplementary Original blot is presented in Supplementary Fig. 1. (**G**) qPCR detection of expression of liver tissue-related factors. (**H**) Western blot detection of Cit-H3 and PAD4 protein expression after DNase-I treatment. Original blot is presented in Supplementary Fig. 2. (**I**) After DNase-I treatment, qPCR was used to detect the expression of related factors. (**J**) Liver injury was detected by TUNEL staining after DNase-I treatment. Data are presented as mean ± SD, n = 5, $^{*}P < 0.05$, $^{**}P < 0.01$, $^{***}P < 0.001$.

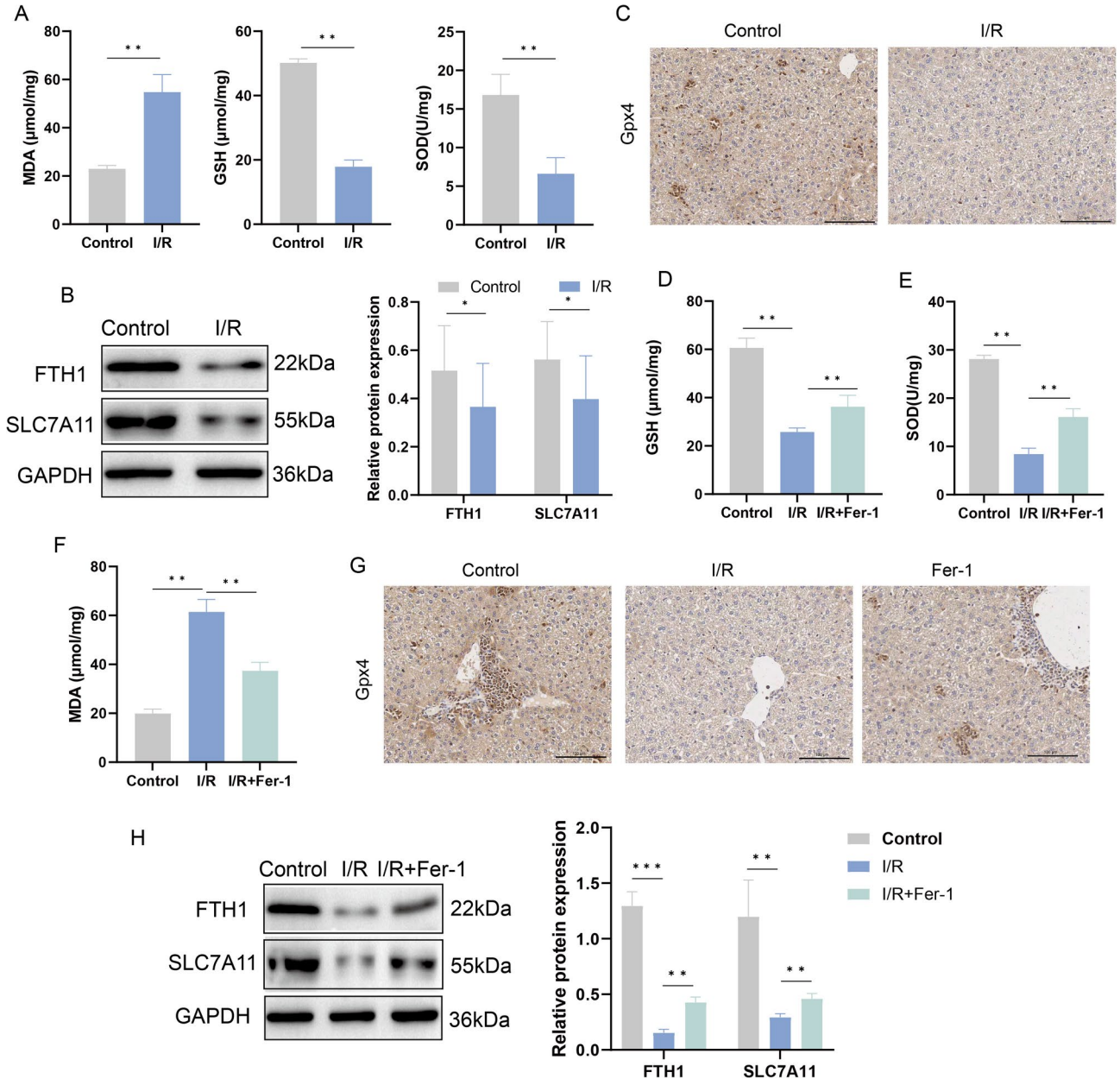

Fig. 2. Ferroptosis-induced NETs promote hepatic I/R injury. (**A**) Detection of GSH, MDA, and SOD levels in mouse liver tissue. (**B**) Western blot analysis of SLC7A11 and FTH1 protein content. Original blot is presented in Supplementary Fig. 3. (**C**) Immunohistochemical detection of GPX4 expression. (**D**–**F**) Detection of GSH, MDA and SOD levels in mouse liver tissue after FER-1 treatment. (**G**) Immunohistochemical detection of GPX4 expression after FER-1 treatment. (**H**) After FER-1 treatment, SLC7A11 and FTH1 protein expression were detected by Western blot. Original blot is presented in Supplementary Fig. 4. Data are presented as mean ± SD, n = 5, $^{*}P < 0.05$, $^{**}P < 0.01$, $^{***}P < 0.001$.

I). Based on the results of the previous experiments, we have known that ferroptosis can induce the formation of NETs. Therefore, we further explored whether knocking down TRIM21 could inhibit this process. The results showed that knockdown of TRIM21 significantly reduced the expression of Cit-H3 and PAD4, as well as the content of MPO (Fig. 4H–K).

TRIM21 regulation of SLC7A11 stability

Through immunofluorescence co-localization experiments, we found a potential interaction between TRIM21 and SLC7A11 (Fig. 5A). Further confirmation of the direct interaction between TRIM21-HA and SLC7A11-FLAG was achieved through CO-IP experiments (Fig. 5B). Finally, ubiquitination assays revealed an increase in the expression of SLC7A11 (Fig. 5C).

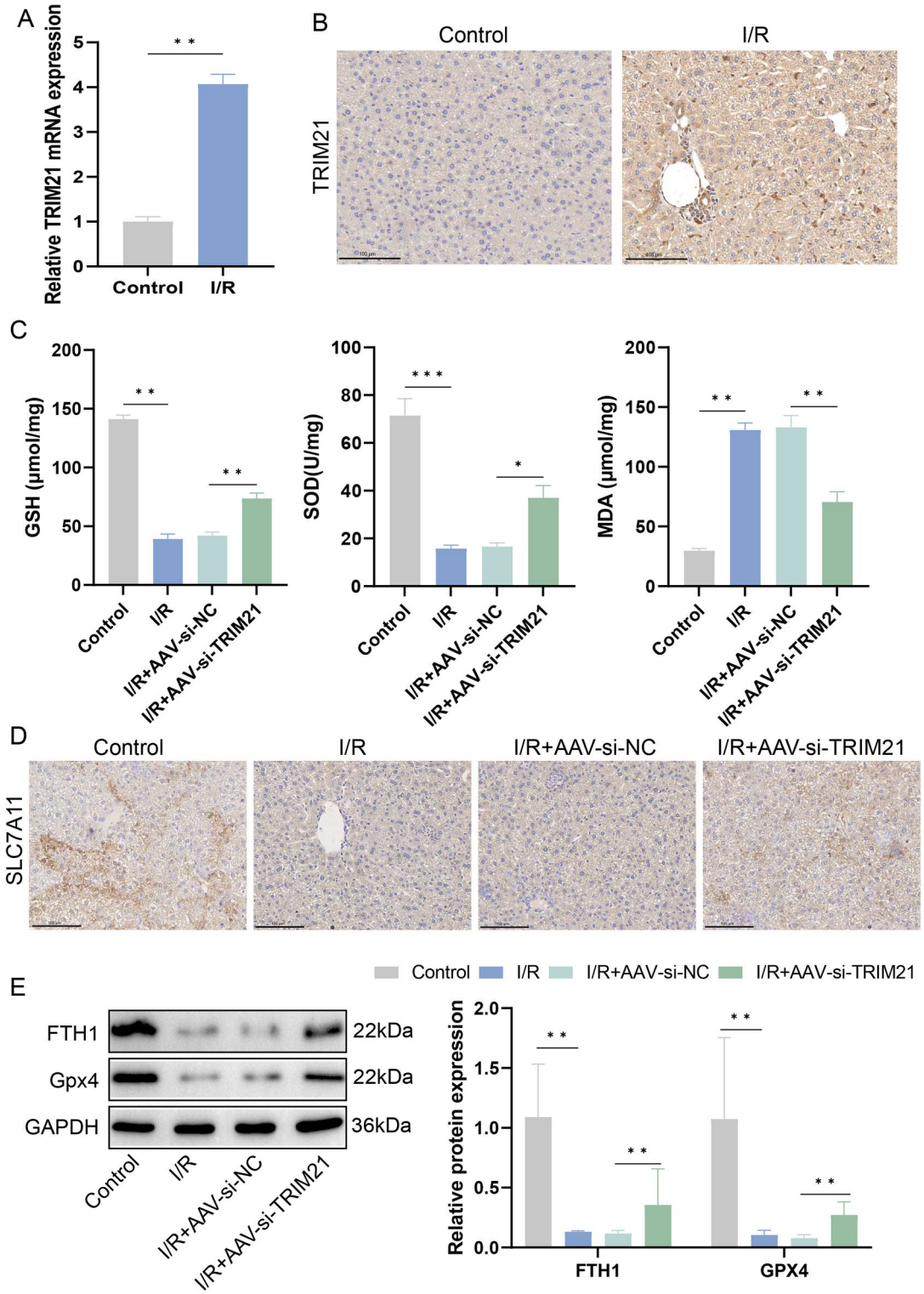

Fig. 3. TRIM21 facilitated the ferroptosis process. (**A**) qPCR detection of TRIM21mRNA expression in mouse liver tissues. (**B**) Immunohistochemistry detection of TRIM21 expression. (**C**) Detection of GSH, MDA and SOD levels in mouse liver tissues after knockdown of TRIM21. (**D**) SLC7A11 expression was detected by immunohistochemistry after knockdown of TRIM21. (**E**) Western blot detection of GPX4 and FTH1 protein expression after knockdown of TRIM21. Original blot is presented in Supplementary Fig. 5. Data are presented as mean ± SD, n = 5, $^{*}P < 0.05$, $^{**}P < 0.01$, $^{***}P < 0.001$.

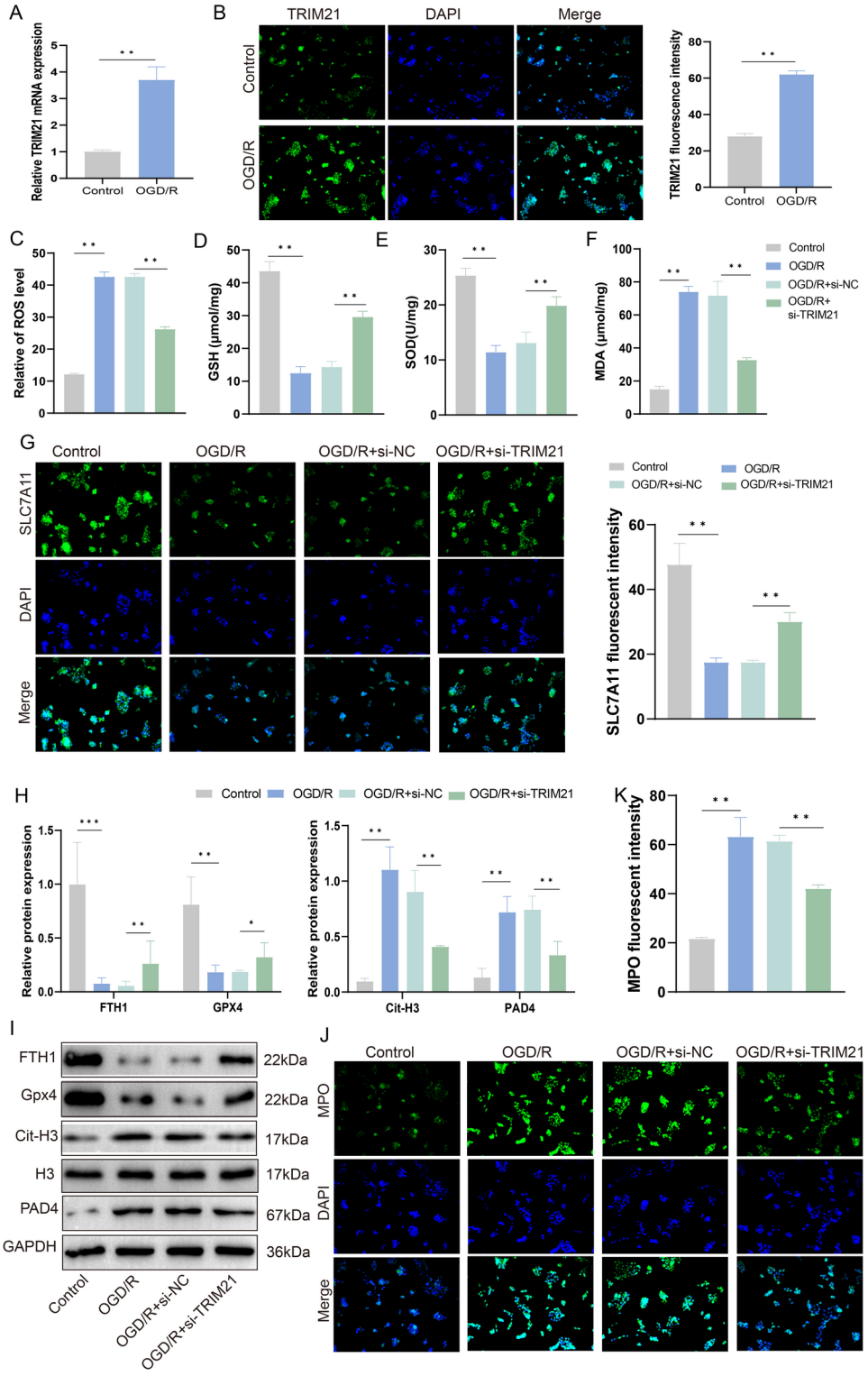

Fig. 4. Knockdown of TRIM21 can inhibit the formation of NETs mediated by ferroptosis in the OGD/R model. (**A**) qPCR detection of TRIM21 mRNA expression in cells. (**B**) Immunofluorescence detection of TRIM21 expression in cells. (**C**) ROS levels were detected in cells after knockdown of TRIM21. (**D**–**F**) Detection of GSH, MDA and SOD levels in cells after knockdown of TRIM21. (**G**) Immunofluorescence detection of SLC7A11 content in cells after knockdown of TRIM21. (**H**–**I**) Western blot detection of GPX4, FTH1, Cit-H3 and PAD4 protein expression in cells after knockdown of TRIM21. Original blot is presented in Supplementary Fig. 6. (**J**–**K**) Immunofluorescence detection of MPO in cells after knockdown of TRIM21. Data are presented as mean ± SD, n = 3, $^{*}P < 0.05$, $^{**}P < 0.01$, $^{***}P < 0.001$.

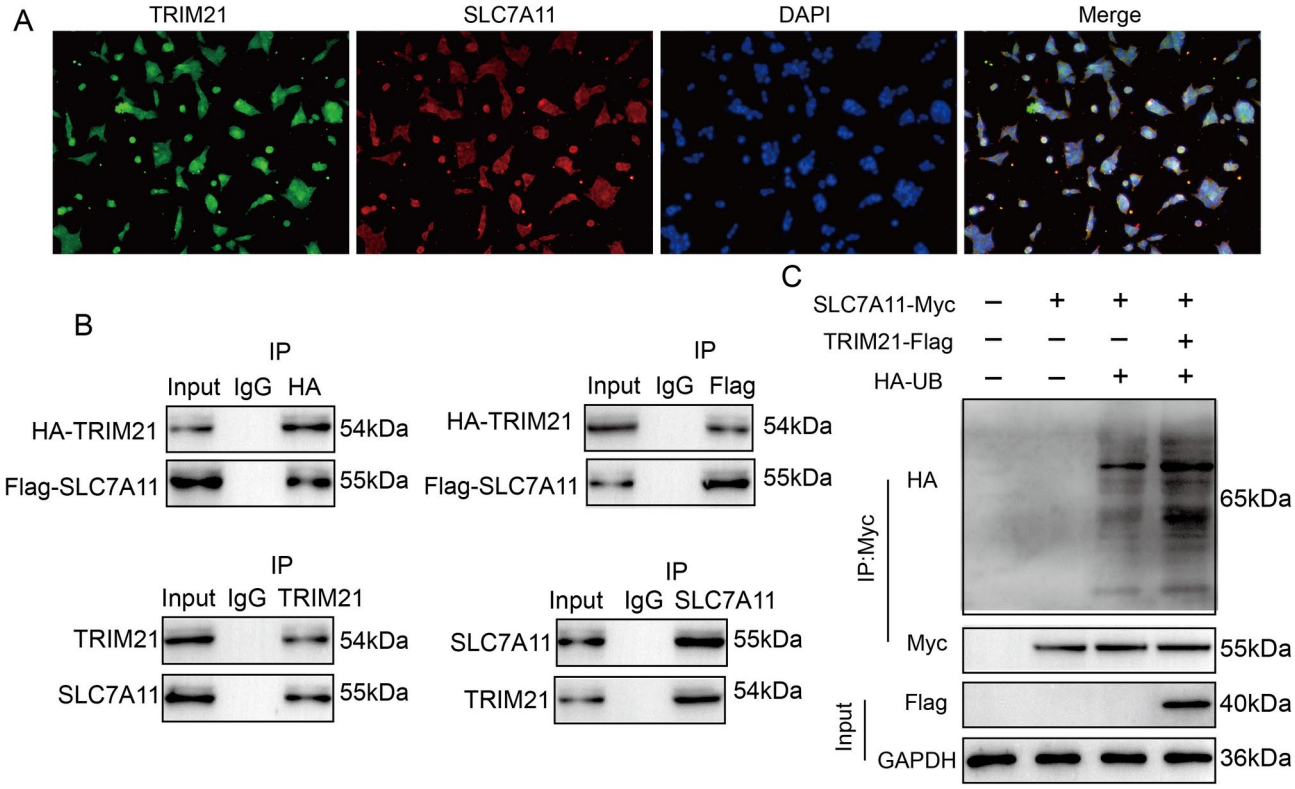

Fig. 5. TRIM21 regulation of SLC7A11 stability. (**A**) immunofluorescence co-localization. (**B**) Co-immunoprecipitation. Original blot is presented in Supplementary Fig. 7. (**C**) Ubiquitination assay. Original blot is presented in Supplementary Fig. 8. Data are presented as mean ± SD, n = 3.

Silencing TRIM21 inhibition of ferroptosis mediates NETs formation to alleviate hepatic I/R injury in vivo

In in vivo studies, by using AAV-mediated si-TRIM21, we explored the potential effects of inhibiting ferroptosis-mediated NETs formation on alleviating hepatic I/R injury. HE staining results indicated that the liver tissue structure in the AAV-si-TRIM21 treatment group was improved, with a reduced degree of liver injury compared to the untreated group (Fig. 6A). Additionally, biochemical assays of serum ALT and AST levels also showed improved liver function (Fig. 6B). TUNEL assays further demonstrated the amelioration of liver injury in the AAV-si-TRIM21 treatment group, with a decrease in apoptosis levels (Fig. 6C). Western blot and immunofluorescence analyses for the expression levels of Cit-H3, PAD4, and MPO showed that the expression of these markers was reduced in the AAV-si-TRIM21 treatment group compared to the control group (Fig. 6D–E). The expression of inflammatory factors such as IL-1β, IL-6, TNF-α, CCL2, CCL5 and CXCL2 was examined by qPCR, and these factors were found to be significantly upregulated in the hepatic I/R injury group but were markedly downregulated in the AAV-si-TRIM21 treatment group. Protein expression of these inflammatory factors was also evaluated, and the results were consistent with the qPCR findings (Fig. 6F–G).

Discussion

In this study, we investigated the role and molecular mechanisms of TRIM21 in hemorrhage-induced hepatic I/R injury. The results revealed that ferroptosis-induced NETs contribute to hepatic I/R injury. In both in vitro and in vivo liver I/R models, the expression of TRIM21 was significantly increased, and the genetic knockout of TRIM21 reduced the formation of ferroptosis-induced NETs, thereby alleviating liver damage. Furthermore, in terms of the molecular mechanism, we found that TRIM21 knockout inhibits the formation of ferroptosis-induced NETs by regulating the stability of SLC7A11 protein, thus mitigating hemorrhage-induced hepatic I/R injury.

Neutrophils form a special structure, known as neutrophil extracellular traps (NETs), in response to infection or injury. NETs consist of DNA, histones, and various antimicrobial proteins, capable of capturing and killing pathogens. However, under pathological conditions, such as in I/R injuries, excessive formation of NETs may exacerbate the inflammatory response and tissue damage. Studies have shown that damage-associated molecular patterns activate neutrophil extracellular traps (NETs), which exacerbate sterile inflammatory liver injury. HMGB1-mediated formation of neutrophil extracellular traps intensifies acute lung injury induced by intestinal ischemia/reperfusion[32–34]. In the results of our study, we found that the expression of NETs formation markers Cit-H3, PAD4, and MPO proteins significantly increased in hepatic I/R injury, indicating that NETs are involved in the process of hepatic I/R injury. In hepatic I/R injury, enhanced intracellular lipid peroxidation during

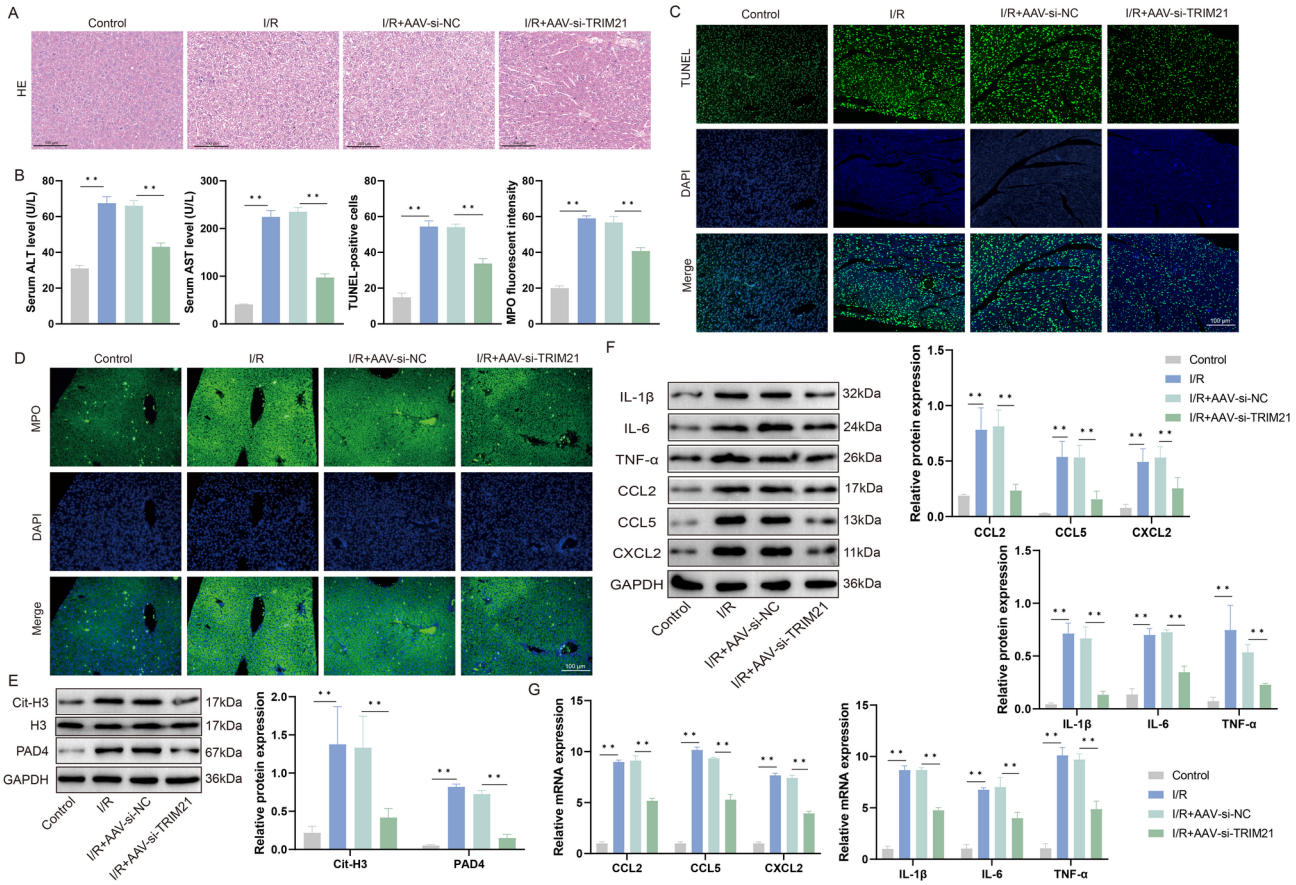

Fig. 6. TRIM21 inhibition of ferroptosis mediates NETs formation to alleviate hepatic I/R injury in vivo. (**A**) HE staining was performed to detect the condition of liver tissue after knockdown of TRIM21. (**B**) Serum levels of ALT and AST were measured after knockdown of TRIM21. (**C**) TUNEL assay for liver injury after knockdown of TRIM21. (**D**) Immunofluorescence detection of MPO in tissues after knockdown of TRIM21. (**E**) Western blot detection of Cit-H3 and PAD4 protein expression in tissues after knockdown of TRIM21. Original blot is presented in Supplementary Fig. 9. (**F**) Western blot detection of related factor expression in tissues after knockdown of TRIM21. Original blot is presented in Supplementary Fig. 10. (**G**) Expression of related factors in tissues was detected by qPCR after knockdown of TRIM21. Data are presented as mean ± SD, n = 5, $^{*}P < 0.05$, $^{**}P < 0.01$, $^{***}P < 0.001$.

ischemia and reperfusion further triggers ferroptosis. As a novel form of programmed cell death, ferroptosis has garnered widespread attention in the study of liver I/R injury in recent years. This process involves the metabolism of iron ions, the regulation of the glutathione (GSH) system, and the disruption of lipid metabolism, which ultimately leads to the rupture of cell membranes and cell death. It has been shown that certain types of cell death, such as ferroptosis and pyroptosis, can induce the formation of NETs. For example, platelet activation and iron death mediate the role of NETosis in heme-induced pulmonary thrombosis. General control of amino acid synthesis by mitochondria 5 like 1 (GCN5L1) promotes the development of nonalcoholic steatohepatitis through ferroptosis-induced formation of extracellular traps in neutrophils. Nonclassical inflammatory vesicle signaling triggers gasdermin D-dependent neutrophil extracellular traps[32,35,36]. However, the relationship between ferroptosis and NETs in hepatic I/R injury is unclear. In this study, we investigated the role of NETs in liver I/R injury and found that the expression of Cit-H3, PAD4 and MPO proteins, which are markers of NETs formation, was significantly increased in the liver I/R injury model. In contrast, the expression of these proteins was suppressed after treatment with DNase I, indicating that the formation of NETs was inhibited. In addition, the formation of NETs induced by ferroptosis further promoted hepatic I/R injury. The results showed that in hepatic I/R injury, ferroptosis markers such as SLC7A11, FTH1, Gpx4 and antioxidant index SOD were significantly decreased in hepatic I/R injury model, and the expression of these indicators was restored after the addition of iron inhibitors. These findings suggest that ferroptosis-induced NETs formation accelerates hepatic I/R injury.

TRIM21 belongs to the TRIM family and is characterized by its distinctive RING domain, which allows it to act as an E3 ubiquitin ligase. In recent years, TRIM21 has been reported to participate in a variety of biochemical processes in the body, including tumorigenesis, pyroptosis, cellular metabolism, and the regulation of oxidative stress[37,38]. However, the role of TRIM21 in ferroptosis remains to be investigated. In this study, we observed significantly elevated levels of TRIM21 in both liver I/R models and OGD/R-induced cellular models. It was

found that the absence of TRIM21 can alleviate doxorubicin-induced cardiotoxicity by inhibiting ferroptosis. TRIM21 promotes the process of ferroptosis by facilitating the ubiquitination and degradation of glutathione peroxidase 4 (GPX4). These discoveries indicate that TRIM21 plays a significant role in cardiac ferroptosis and may serve as a potential therapeutic target for heart disease[28,39]. Consequently, we explored whether TRIM21 promotes the process of ferroptosis. Our results demonstrated that the knockdown of TRIM21 upregulated the expression of iron markers SLC7A11, Gpx4, FTH1, SOD and GSH, while simultaneously suppressing the expression of MDA. These findings confirm that TRIM21 promotes the occurrence of ferroptosis. SLC7A11 is a key marker in the process of ferroptosis. Some studies have found that the ferroptosis process can be influenced by regulating the ubiquitination of SLC7A11. For instance, mesenchymal stem cells prevent ferroptosis in acute liver injury through the stabilization of SLC7A11 mediated by exosomes. SOCS2 promotes ferroptosis and radiosensitization in hepatocellular carcinoma by enhancing the ubiquitination of SLC7A11[40–42]. Consistent with these findings, our research discovered that[41]. TRIM21 influences the process of ferroptosis by ubiquitinating SLC7A11. Furthermore, given the role of ferroptosis-induced NETs formation in hepatic I/R injury as indicated by previous studies, we further explored the impact of TRIM21 on ferroptosis-induced NETs formation in hepatic I/R injury. The study results showed that in both in vivo liver I/R and in vitro OGD/R-induced hepatocyte models, the knockdown of TRIM21 promoted the expression of iron markers SLC7A11, Gpx4, FTH1, and SOD, and inhibited the expression of Cit-H3, PAD4, and MPO, suggesting that the knockdown of TRIM21 could suppress the formation of NETs induced by ferroptosis, thereby alleviating hepatic I/R injury.

Conclusions

In summary, our study has revealed that TRIM21 knockdown inhibits ferroptosis-induced NETs formation by regulating the stability of SLC7A11, thereby alleviating hemorrhage-induced liver I/R injury. This provides a potential therapeutic strategy for mitigating hemorrhage-induced liver damage.

Data availability

The data that support the findings of this study are available from the corresponding author upon reasonable request.

Received: 19 December 2024; Accepted: 17 April 2025
Published online: 14 May 2025

References

1. Zhou, H. et al. Remote ischemic preconditioning attenuates hepatic ischemia/reperfusion injury after hemorrhagic shock by increasing autophagy. *Int. J. Med. Sci.* **18**, 873–882. https://doi.org/10.7150/ijms.51268 (2021).
2. Paxian, M., Bauer, I., Kaplan, D., Bauer, M. & Rensing, H. Hepatic redox regulation of transcription factors activator protein-1 and nuclear factor-kappaB after hemorrhagic shock in vivo. *Antioxid. Redox Signal.* **4**, 711–720. https://doi.org/10.1089/152308602760598855 (2002).
3. Tong, G. et al. FGF18 alleviates hepatic ischemia-reperfusion injury via the USP16-mediated KEAP1/Nrf2 signaling pathway in male mice. *Nat. Commun.* **14**, 6107. https://doi.org/10.1038/s41467-023-41800-x (2023).
4. Du, S. et al. Hepatocyte HSPA12A inhibits macrophage chemotaxis and activation to attenuate liver ischemia/reperfusion injury via suppressing glycolysis-mediated HMGB1 lactylation and secretion of hepatocytes. *Theranostics* **13**, 3856–3871. https://doi.org/10.7150/thno.82607 (2023).
5. Liu, L. et al. Hepatocyte-derived extracellular vesicles miR-122-5p promotes hepatic ischemia reperfusion injury by regulating Kupffer cell polarization. *Int. Immunopharmacol.* **119**, 110060. https://doi.org/10.1016/j.intimp.2023.110060 (2023).
6. Lin, J. et al. Quercetin, a natural flavonoid, protects against hepatic ischemia-reperfusion injury via inhibiting Caspase-8/ASC dependent macrophage pyroptosis. *J. Adv. Res.* https://doi.org/10.1016/j.jare.2024.05.010 (2024).
7. Liu, R. et al. ZBP1-mediated apoptosis and inflammation exacerbate steatotic liver ischemia/reperfusion injury. *J. Clin. Invest.* https://doi.org/10.1172/jci180451 (2024).
8. Antipenko, S. et al. Neutrophils are indispensable for adverse cardiac remodeling in heart failure. *J. Mol. Cell. Cardiol.* **189**, 1–11. https://doi.org/10.1016/j.yjmcc.2024.02.005 (2024).
9. Li, Z. & Lu, Q. The role of neutrophils in autoimmune diseases. *Clin. Immunol.* **266**, 110334. https://doi.org/10.1016/j.clim.2024.110334 (2024).
10. Wang, Y., Du, C., Zhang, Y. & Zhu, L. Composition and function of neutrophil extracellular traps. *Biomolecules* https://doi.org/10.3390/biom14040416 (2024).
11. Zeineddine, H. A. et al. Neutrophils and neutrophil extracellular traps cause vascular occlusion and delayed cerebral ischemia after subarachnoid hemorrhage in mice. *Arterioscler. Thromb. Vasc. Biol.* **44**, 635–652. https://doi.org/10.1161/atvbaha.123.320224 (2024).
12. Wu, X. & Yang, Y. Neutrophil extracellular traps (NETs) and fibrotic diseases. *Int. Immunopharmacol.* **133**, 112085. https://doi.org/10.1016/j.intimp.2024.112085 (2024).
13. Du, X. et al. PRL2 regulates neutrophil extracellular trap formation which contributes to severe malaria and acute lung injury. *Nat. Commun.* **15**, 881. https://doi.org/10.1038/s41467-024-45210-5 (2024).
14. Salzmann, M. et al. Neutrophil extracellular traps induce persistent lung tissue damage via thromboinflammation without altering virus resolution in a mouse coronavirus model. *J. Thromb. Haemost.* **22**, 188–198. https://doi.org/10.1016/j.jtha.2023.09.014 (2024).
15. Liu, B. et al. Neutrophil extracellular traps promote intestinal barrier dysfunction by regulating macrophage polarization during trauma/hemorrhagic shock via the TGF-β signaling pathway. *Cell. Signal.* **113**, 110941. https://doi.org/10.1016/j.cellsig.2023.110941 (2024).
16. Brunnthaler, L. et al. Intrahepatic neutrophil accumulation and extracellular trap formation are associated with posthepatectomy liver failure. *Hepatol. Commun.* https://doi.org/10.1097/hc9.0000000000000348 (2024).
17. Liu, X. et al. Gene regulation of neutrophils mediated liver and lung injury through NETosis in acute pancreatitis. *Inflammation* https://doi.org/10.1007/s10753-024-02071-w (2024).
18. Liu, G. et al. Ferroptosis in cardiovascular disease. *Biomed. Pharmacother.* **170**, 116057. https://doi.org/10.1016/j.biopha.2023.116057 (2024).
19. Xiang, Q., Yi, X., Zhu, X. H., Wei, X. & Jiang, D. S. Regulated cell death in myocardial ischemia-reperfusion injury. *Trends Endocrinol. Metab.* **35**, 219–234. https://doi.org/10.1016/j.tem.2023.10.010 (2024).

20. Chen, Y. et al. Cpd-A1 alleviates acute kidney injury by inhibiting ferroptosis. *Acta Pharmacol. Sin.* **45**, 1673–1685. https://doi.org/10.1038/s41401-024-01277-w (2024).
21. Zuo, Z. et al. Selenium nanoparticles alleviate renal ischemia/reperfusion injury by inhibiting ferritinophagy via the XBP1/NCOA4 pathway. *Cell Commun. Signal.* **22**, 376. https://doi.org/10.1186/s12964-024-01751-2 (2024).
22. Jia, K. W. et al. Interferon-α stimulates DExH-box helicase 58 to prevent hepatocyte ferroptosis. *Mil. Med. Res.* **11**, 22. https://doi.org/10.1186/s40779-024-00524-9 (2024).
23. Han, L. et al. AhR-STAT3-HO-1/COX-2 signalling pathway may restrict ferroptosis and improve hMSC accumulation and efficacy in mouse liver. *Br. J. Pharmacol.* **181**, 125–141. https://doi.org/10.1111/bph.16208 (2024).
24. Rajsbaum, R., García-Sastre, A. & Versteeg, G. A. TRIMmunity: The roles of the TRIM E3-ubiquitin ligase family in innate antiviral immunity. *J. Mol. Biol.* **426**, 1265–1284. https://doi.org/10.1016/j.jmb.2013.12.005 (2014).
25. Li, Z. et al. TRIM21 aggravates cardiac injury after myocardial infarction by promoting M1 macrophage polarization. *Front. Immunol.* **13**, 1053171. https://doi.org/10.3389/fimmu.2022.1053171 (2022).
26. Qu, Z. et al. The positive feedback loop of the NAT10/Mybbp1a/p53 axis promotes cardiomyocyte ferroptosis to exacerbate cardiac I/R injury. *Redox Biol.* **72**, 103145. https://doi.org/10.1016/j.redox.2024.103145 (2024).
27. Zeng, Y. et al. Baicalin-peptide supramolecular self-assembled nanofibers effectively inhibit ferroptosis and attenuate doxorubicin-induced cardiotoxicity. *J. Control Release* **366**, 838–848. https://doi.org/10.1016/j.jconrel.2023.12.034 (2024).
28. Hou, K. et al. Loss of TRIM21 alleviates cardiotoxicity by suppressing ferroptosis induced by the chemotherapeutic agent doxorubicin. *EBioMedicine* **69**, 103456. https://doi.org/10.1016/j.ebiom.2021.103456 (2021).
29. Gong, J. et al. TRIM21-promoted FSP1 plasma membrane translocation confers ferroptosis resistance in human cancers. *Adv. Sci. (Weinh)* **10**, e2302318. https://doi.org/10.1002/advs.202302318 (2023).
30. Wang, M. et al. Moxibustion-mediated alleviation of synovitis in rats with rheumatoid arthritis through the regulation of NLRP3 inflammasome by modulating neutrophil extracellular traps. *Heliyon* **10**, e23633. https://doi.org/10.1016/j.heliyon.2023.e23633 (2024).
31. Zeng, F. L. et al. Neutrophil extracellular traps promote acetaminophen-induced acute liver injury in mice via AIM2. *Acta Pharmacol. Sin.* **45**, 1660–1672. https://doi.org/10.1038/s41401-024-01239-2 (2024).
32. Zhao, Q. et al. NK-cell-elicited gasdermin-D-dependent hepatocyte pyroptosis induces neutrophil extracellular traps that facilitate HBV-related acute-on-chronic liver failure. *Hepatology* https://doi.org/10.1097/hep.0000000000000868 (2024).
33. Yili, S. et al. Activation of GPR81 aggravated intestinal ischemia/reperfusion injury-induced acute lung injury via HMGB1-mediated neutrophil extracellular traps formation. *Int. J. Immunopathol. Pharmacol.* **37**, 3946320231193832. https://doi.org/10.1177/03946320231193832 (2023).
34. Bork, F. et al. naRNA-LL37 composite DAMPs define sterile NETs as self-propagating drivers of inflammation. *EMBO Rep.* **25**, 2914–2949. https://doi.org/10.1038/s44319-024-00150-5 (2024).
35. Abrams, S. T. et al. Damage-associated cellular markers in the clinical and pathogenic profile of vaccine-induced immune thrombotic thrombocytopenia. *J. Thromb. Haemost.* **22**, 1145–1153. https://doi.org/10.1016/j.jtha.2023.12.008 (2024).
36. Lv, T. et al. Mitochondrial general control of amino acid synthesis 5 like 1 promotes nonalcoholic steatohepatitis development through ferroptosis-induced formation of neutrophil extracellular traps. *Clin. Transl. Med.* **13**, e1325. https://doi.org/10.1002/ctm2.1325 (2023).
37. Huang, Y., Gao, X., He, Q. Y. & Liu, W. A interacting model: How TRIM21 orchestrates with proteins in intracellular immunity. *Small Methods* **8**, e2301142. https://doi.org/10.1002/smtd.202301142 (2024).
38. Huang, H. et al. LANCL1, a cell surface protein, promotes liver tumor initiation through FAM49B-Rac1 axis to suppress oxidative stress. *Hepatology* **79**, 323–340. https://doi.org/10.1097/hep.0000000000000523 (2024).
39. Sun, X. et al. TRIM21 ubiquitylates GPX4 and promotes ferroptosis to aggravate ischemia/reperfusion-induced acute kidney injury. *Life Sci.* **321**, 121608. https://doi.org/10.1016/j.lfs.2023.121608 (2023).
40. Wang, Z. et al. TRIM3 facilitates ferroptosis in non-small cell lung cancer through promoting SLC7A11/xCT K11-linked ubiquitination and degradation. *Cell Death Differ.* **31**, 53–64. https://doi.org/10.1038/s41418-023-01239-5 (2024).
41. Wang, J., Jia, Q., Jiang, S., Lu, W. & Ning, H. POU6F1 promotes ferroptosis by increasing lncRNA-CASC2 transcription to regulate SOCS2/SLC7A11 signaling in gastric cancer. *Cell Biol. Toxicol.* **40**, 3. https://doi.org/10.1007/s10565-024-09843-y (2024).
42. Lin, F. et al. Mesenchymal stem cells protect against ferroptosis via exosome-mediated stabilization of SLC7A11 in acute liver injury. *Cell Death Dis.* **13**, 271. https://doi.org/10.1038/s41419-022-04708-w (2022).

Acknowledgements
We thank all the members of the department.

Author contributions
1—Conceived and designed the experiments: XSC 2—Performed the experiments: ZPL, SKW and XSC 3—Analyzed and interpreted the data: SKW, YXC and DH 4—Contributed reagents, materials, analysis tools or data: ZPL and KD 5—Wrote the paper: SKW.

Funding
This research was supported by the Shenzhen Basic Research Project (No. JCYJ20210324112014040), Shenzhen Nanshan District Health System Science and Technology Major Project (No. NSZD2023045, No. NSZD2023001, NO. NSZD2024008), Hospital project of Union Shenzhen Hospital of Huazhong University of Science and Technology (NO. YN2022020), Shenzhen Nanshan District science and technology plan key project (NO. NS2024013, No. 2020005).

Declarations

Competing interests
The authors declare no competing interests.

Ethics approval and consent to participate
Animal experiments were approved by the Ethics Committee of Nanshan people's hospital.

Informed consent
There are no human subjects in this article, and informed consent is not applicable.

Additional information

Supplementary Information The online version contains supplementary material available at https://doi.org/10.1038/s41598-025-99182-7.

Correspondence and requests for materials should be addressed to X.C.

Reprints and permissions information is available at www.nature.com/reprints.

Publisher's note Springer Nature remains neutral with regard to jurisdictional claims in published maps and institutional affiliations.